WPJET1-PR(17) 17153

D Van Eester et al.

The effect of wave interference in the three-ion" ion cyclotron resonance heating scheme"

Preprint of Paper to be submitted for publication in
Plasma Physics and Controlled Fusion

This work has been carried out within the framework of the EUROfusion Consortium and has received funding from the Euratom research and training programme 2014-2018 under grant agreement No 633053. The views and opinions expressed herein do not necessarily reflect those of the European Commission.

The effect of wave interference in the "three-ion" ion cyclotron resonance heating scheme

D. Van Eester, Ye.O. Kazakov & E.A. Lerche
Laboratorium voor Plasmafysica - Laboratoire de Physique des Plasmas
Belgian EUROfusion Consortium Member
Trilateral Euregio Cluster
Renaissancelaan 30 Avenue de la Renaissance
B-1000, Brussels, Belgium

January 30, 2017

Abstract

The "3-ion scheme" [Ye.O. Kazakov et al., *Nucl. Fusion* **55** (2015) 032001] is a new, high potential ion cyclotron resonance heating (ICRH) scheme that has recently been proposed and experimentally tested. In this paper a simple cold-plasma analytical model is introduced, which shows the beneficial effect of wave interference on the efficiency of wave damping in a plasma for this scenario. Furthermore, we show the changes of wave polarisation brought about by a tiny third minority when added to 2 majority ion species are favourable for damping wave power on minority ions.

1 Introduction

Classical "minority" heating at the fundamental cyclotron layer adopts a minority immersed in a majority plasma to make essential changes to the wave polarisation brought about by the nearby confluence layer and allowing to overcome the screening the plasma sets up at the cyclotron layer when trying to heat a single ion species. For not too energetic particles, fundamental ion cyclotron resonance heating relies on the (E_+) wave polarisation component rotating in the sense of the ion cyclotron oscillation to ensure efficient transfer of energy from the waves to the plasma; only for energetic particles comes the component rotating in the sense of the electrons (E_-) non-negligibly into play. At the mode conversion point were the fast wave has a confluence with the (electrostatic) Bernstein mode, the wave

electrostatic component is locally more prominent. Recently, the philosophy of minority heating was extended to a scheme that is efficient at much smaller concentrations than the usual minority heating (see e.g. [1, 2]). As it involves a minimum of 3 ions, it is known as the "3-ion scheme". Two of the ions species usually - but not necessarily - are majorities, and a third that is a minority which only is present in minute amounts. The charge-to-mass ratio of the minority needs to lie in between the charge-to-mass ratios of the majorities. After having been identified as having a good heating potential based on predictive kinetic modelling, the scheme was successfully exploited experimentally (see e.g. [3, 4, 5]). In JET and Alcator C-Mod experiments, adding a small amount of ^{3}He minority ions ($< 1\%$) was demonstrated to be sufficient for effective heating of H-D plasma mixtures.

The three-ion D-(^{3}He)-H minority scenario is closely linked to the earlier minority and mode conversion heating in (^{3}He)-H JET plasmas, which was equipped with carbon wall. Indeed, as discussed in detail in [6], the presence of intrinsic carbon impurities and residual D-like species resulted in the appearance of the second mode conversion layer in a plasma. The presence of two mode conversion layers rather than a single one resulted in constructive/destructive wave interference, which occurs due to the partial reflection of the incident wave at every MC layer. Taking into account wave interference effect allowed to explain the observed heating efficiencies in (^{3}He)-H JET-C experiments. As noted in [1], the effect of wave interference also plays a role in the 3-ion scheme, when most of RF power is absorbed by a small amount of resonant minority. The modest goal of the present paper is to build a cold-plasma model, which allows to quantify in more detail the wave interference and polarisation changes in the vicinity of mode conversion layers in the 3-ion scheme. We note that a hot plasma description is required in order to distinguish the power transfer from the waves to electrons (as in case of mode conversion heating experiments) and to minority ions (as in case of 3-ion scenario).

Apart from the introduction, this text is subdivided in 5 sections and an appendix. Section 2 provides a quantitative example of the scheme. Section 3 is devoted to deriving appropriate simplified equations allowing to study the 3-ion scheme analytically. The basic ingredients being resonances and cutoffs, the next section (section 4) briefly discusses the asymptotic solutions of the Budden and the Airy equation and then proceeds to computing the global connection coefficients across the whole region of interest. In the next but last section (section 5) it is shown that highly localised damping gives rise to wave reflection. In section 6, finally, the conclusions are summarised. Some details on the asymptotic solution of the relevant equations are provided in the Appendix.

2 Quantitative example of the 3-ion scheme

Prior to studying the underlying physics, this section provides an example of the potential of the 3-ion scheme. The adopted parameters are typical for JET. Hydrogen and deuterium are the majority species and fundamental cyclotron heating of a small amount of helium-

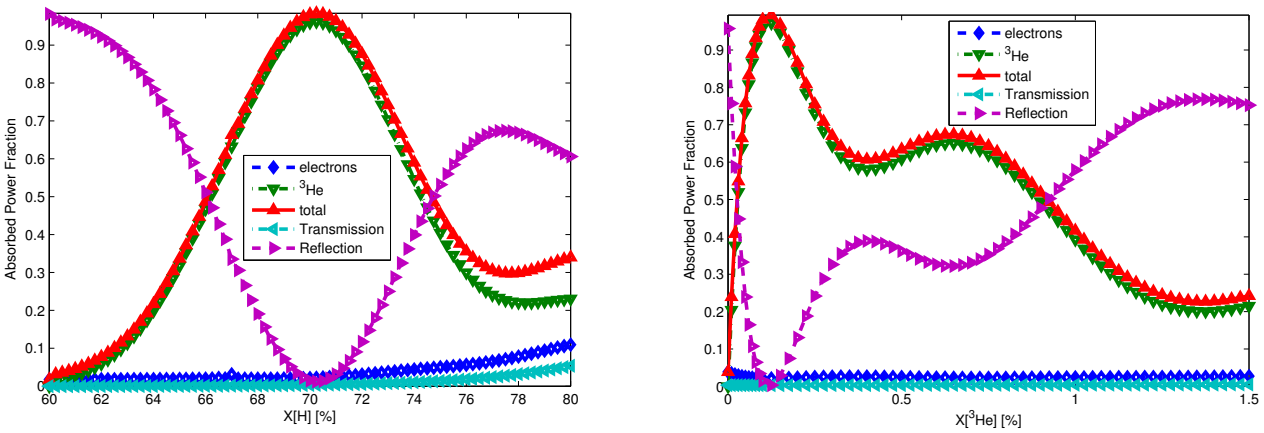

Figure 1: Double transit absorption and connection coefficients for a fast wave launched from the low field side in a $D-(^3He)-H$ plasma: hydrogen majority scan (left) and ^3He minority scan (right) concentration scan.

3 is aimed at. The major and minor radii are $R_o = 2.97m$ and $a_p = 0.95m$. A central density of $N_{eo} = 5 \times 10^{19}/m^3$ and a temperature of $T_{eo} = T_{io} = 4keV$ are considered. At the edge these values reduce to $N_{es} = 10^{19}/m^3$ and $T_{es} = T_{is} = 10eV$. The adopted density and temperature profile factors are 1 and 1.5, respectively. For central fundamental cyclotron heating of the ^3He minority the adopted RF driver frequency is $33MHz$ with a magnetic field strength of $3.31T$. Figure 1 depicts the absorption for a fast wave incident from the low field side, as well as the corresponding reflection and transmission coefficients. The integration interval is $-0.5m < x < +0.5m$ where x is the distance with respect to the geometric axis in the equatorial plane. As discussed by Kazakov [2], the 3-ion scheme requires a specific mix of the majority ions and fairly small minority concentrations. For the adopted D-(^{3}He)-H scenario, a crude guess ignoring the effect of the finite parallel wave number requires $X[H] \approx 2/3$ and $X[^3He] < 1\%$; accounting for $k_{//}$ increases the hydrogen minority value slightly to $X[H] \approx 70\%$. Under the considered coditions, the absorption is close to 100% and the ^3He minority is the only significant absorber.

Figure 2 depicts 2 absorption and wave polarisation profiles; the specific parameters $X[H] = 66\%$ (slightly under the concentration guaranteeing optimal absorption) and $X[H] = 70\%$ (optimal concentration for maximising the ^3He minority heating) are chosen; $X[^3He] = 0.1\%$. The subscripts R and x refer to the direction along the major radius $R = R_o + x$ ($E_x = E_R = \vec{E}.\vec{e}_R$) while $\vec{e}_y$ is perpendicular to $\vec{e}_x$ in a toroidal cut; $E_\pm = E_x \pm iE_y$. The magnitude of the E_+ wave field component rotating with the ions and responsible for ion heating peaks close to the location where the absorption is maximal. It can be seen that the poloidal (E_y) component is very small on the high field side of the absorption layer while the the short wavelength electrostatic component is large at the ion-ion hybrid layer corresponding to the pair of majority ions which lies just to the left of $\omega = \Omega_{^3He}$, suggesting that the nearby ion-ion hybrid layer due to the presence of the 2 majorities has an impact on the wave-particle interaction.

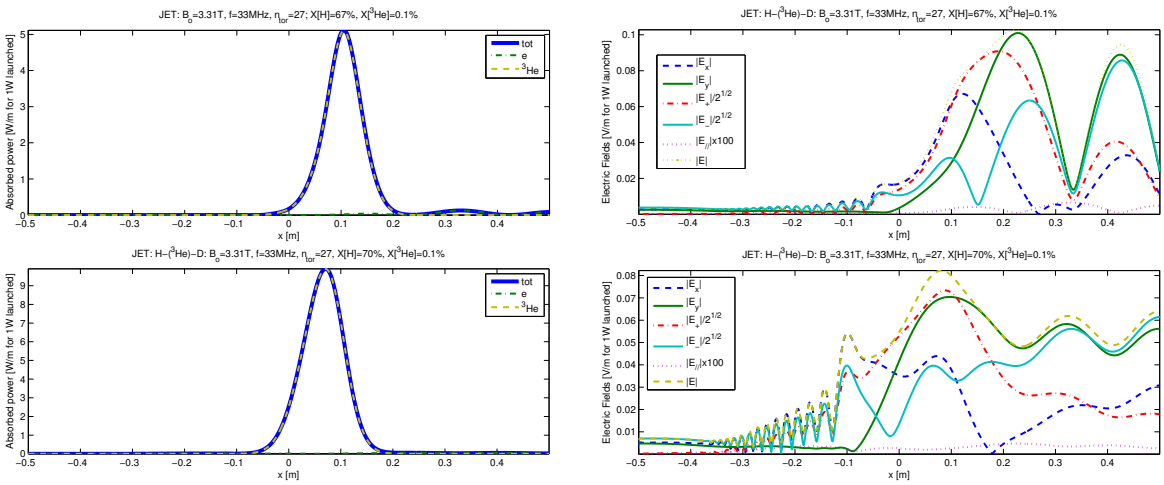

Figure 2: Absorption (left) and wave polarisation (right) profile for a hydrogen majority concentration of $X[H] = 66\%$ (top) and $X[H] = 70\%$ (bottom). The minority concentration is $X[^3He] = 0.1\%$; its ^3He cyclotron layer is at $x \approx 0.06m$.

3 Evaluation of a proper simplified expression of the wave equation coefficients

The cold plasma wave equation can be written [7]

$$\nabla \times \nabla \times \vec{E} = k_o^2 \overline{\overline{K}}.\vec{E}$$

where - aligning the z-direction with the direction parallel to the static magnetic field -

$$\overline{\overline{K}} = \begin{pmatrix} S_{Stix} & -iD_{Stix} & 0 \\ +iD_{Stix} & S_{Stix} & 0 \\ 0 & 0 & P_{Stix} \end{pmatrix}$$

in which S_{Stix}, D_{Stix} and P_{Stix} are provided e.g. by Stix and $k_o = \omega/c$; $\omega = 2\pi f$ where f is the driver frequency and c is the speed of light. S_{Stix} and D_{Stix} are typically decomposed into the terms responsible for the left and right hand circular motion: $S_{Stix} = (R_{Stix} + L_{Stix})/2$ and $D_{Stix} = (R_{Stix} - L_{Stix})/2$. Here

$$R_{Stix} = 1 - \sum_\beta \frac{\omega_{p,\beta}^2}{\omega(\omega + \Omega_\beta)}$$

$$L_{Stix} = 1 - \sum_\beta \frac{\omega_{p,\beta}^2}{\omega(\omega - \Omega_\beta)}.$$

In the above, $\omega_{p,\beta}$ is the plasma and Ω_β the cyclotron frequency of the species β. Ion cyclotron heating typically relies on the fast magnetosonic wave to propagate the wave energy from the launcher outside the main plasma to the core of the tokamak plasma. As the fast wave has a negligible parallel electric field ("parallel" and "perpendicular" are w.r.t. the static magnetic field direction), it will simply be assumed to be zero in this text. It is further assumed that the only inhomogeneities of the density and the magnetic field lie in the x-direction so that the y- and z- coordinates are ignorable i.e. that the field is composed or independent components proportional to $exp[i(k_y y + k_z z)]$. Further more we assume that k_y can be taken zero and that the parallel wave number $k_z = k_{//}$ is known is prescribed; the distinction between the parallel and the toroidal direction is ignored. The relevant wave equation now only involves the y-component of the electric field. The other perpendicular component is not small but can be found once E_y is known. The fast-wave-only wave equation is

$$\frac{dE_y^2}{d^2x} + k_{\perp,FW}^2 E_y = 0$$

where

$$k_{\perp,FW}^2 = \frac{(k_o^2 R_{Stix} - k_{//}^2)(k_o^2 L_{Stix} - k_{//}^2)}{k_o^2 S - k_{//}^2}.$$

The electric field component in the direction of the inhomogeneity is directly obtained from the first component of the vectorial wave equation:

$$E_x = \frac{i k_o^2 D_{Stix}}{k_o^2 S_{Stix} - k_{//}^2} E_y$$

Note that this component goes through a maximum at the resonance; this is the cold plasma equivalent of the earlier shown electrostatic component reaching a maximum at the mode conversion layer. In a hot plasma, the damping is described via the Fried-Conte plasma dispersion function $Z_{FC}(\zeta)$ [8]; in the above it suffices to make the replacement

$$\frac{1}{\omega \pm \Omega_\beta} \rightarrow -\frac{1}{2^{1/2} k_{//} v_{th,\beta}} Z_{FC}\left(\frac{\omega \pm \Omega}{2^{1/2} k_{//} v_{th,\beta}}\right)$$

in which $v_{th,\beta}$ is the thermal velocity. We will be using an approximate rather than the actual reigning wave equation; the coefficients of the approximate equation will be evaluated close to the region of interest using a Taylor series expansion truncated at the linear terms. The Fried-Conte function cannot be represented by an equation that only has linear coefficients. Its dependence can however be approximated in a simply way without requiring to extend the

polynomial order of the coefficients, introducing finite collisionality by adding a small imaginary part to the driver frequency ($\omega \rightarrow \omega + i\nu$). For vanishingly small ν and when the width of the damping region is small w.r.t. the machine's major radius so that the approximation $B_o = B_{00}/(1+x/R_o) \approx B_{00}(1-x/R_o)$ can be adopted, the integral through the fundamental cyclotron damping region yields the same result ($\pi R(x_{min})/\omega$) in both cases. Although the shape is slightly different, adopting a suitable ν allows to get a reasonable match. Imposing the slope at $\omega = \Omega_{min}$ to be identical requires $\nu = k_{//} v_{th,\min}$ while matching the maximal value of the real part requires $\nu = k_{//} v_{th,min}/[2^{1/2} Re[Z_{FC}]_{max}]$ in which $Re[Z_{FC}]_{max} \approx 1.08$. In both cases ν/ω is the order of 1% for the earlier adopted experimental parameters. Although not fully rigorous, this simplification has the advantage that all the coefficients of the differential equation are now linear. Note that the size of the collisional correction is bigger than the correction obtained from Coulomb collisions, the latter typically being 6 orders of magnitude smaller than the driver frequency in hot fusion relevant plasmas. Nevertheless it is still a very modest correction: the Budden equations's wavelength being $6m$ and relevant η being of order 1 (see further; $\eta = k_\infty \Delta x$ where $k_\infty \approx 25 - 50/m$).

Once the solution of the wave equation is known, one can evaluate the left and right rotating components of the electric field: $E_\pm = E_x \pm i E_y$. Note that the fraction E_+/E_- does not even involve evaluating E_y as it suffices to use a normalised version of it:

$$\frac{E_+}{E_-} = -\frac{k_o^2 R_{Stix} - k_{//}^2}{k_o^2 L_{Stix} - k_{//}^2}$$

Looking at the expression for the dispersion root, it is clear that $|E_+/E_-|$ is maximised at the $k_o^2 L - k_{//}^2$ cutoff point. Also note that the fast wave has a resonance at $k_o^2 S_{Stix} = k_{//}^2$ and hence is rapidly varying there. While R_{Stix} is only mildly varying, L_{Stix} passes through infinity at the minority cyclotron layers $\omega = \Omega_\beta$. The 3-ion scheme aims at exploiting the cyclotron frequency of the minority and hence the majority cyclotron layers are commonly at some distance from the region where the minority absorbs. Note that the contributions from the 2 majorities to L_{Stix} are of opposite sign so that the one partly compensates the other. One of the basic features of the 3-ion scheme is to ensure the local annihilation of $k_o^2 L_{Stix} - k_{//}^2$. Since $|k_o^2 L_{Stix}|$ is typically much larger than $|k_{//}^2|$, this essentially requires to balance the 2 majority contributions. The remaining (minority) term having a resonant denominator, its contributions are significant close to the cyclotron resonance, even at modest minority concentration. Figure 3 shows a typical polarization.

We will now find a suitable simplified version of the reigning differential equation. As the damping the 3-ion scheme relies on is at the fundamental cyclotron frequency of the minority, the simplified equation should provide a fair representation near that layer. Since the R varies only mildly, it can be approximated by its value at the minority cyclotron position x_{min}. For the L term, a similar procedure can be used, except for the minority term. For the latter the function in the numerator can replaced by its value at the cyclotron position, and for the denominator a Taylor series expansion of the cyclotron frequency truncated at the linear

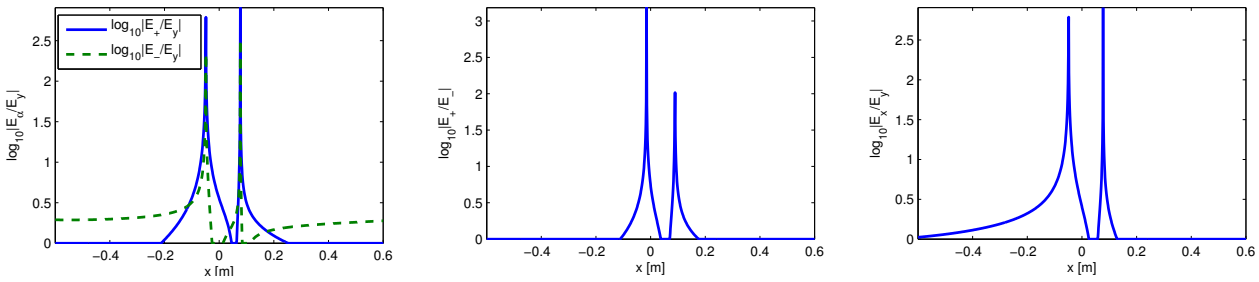

Figure 3: Typical polarisation for the 3-ion scheme; parameters as discussed earlier.

term is used. One gets

$$R_{Stix} \approx 1 - \sum_{\beta:e,maj,min} \frac{\omega_{p,\beta}^2(x_{min})}{\omega[\omega + \Omega_\beta(x_{min})]}$$

$$L_{Stix} \approx 1 - \sum_{\beta:e,maj} \frac{\omega_{p,\beta}^2(x_{min})}{\omega[\omega - \Omega_\beta(x_{min})]} - \frac{\omega_p^2(x_{min})}{\omega^2} \frac{R_{min}}{x + i\nu R_{min}/\omega}$$

where Ω_{min} was substituted by ω. Figure 4 gives an idea of the variation of R and L in the region of interest, adopting parameters as chosen before. Linear approximations are sufficiently accurate close to the cyclotron layer.

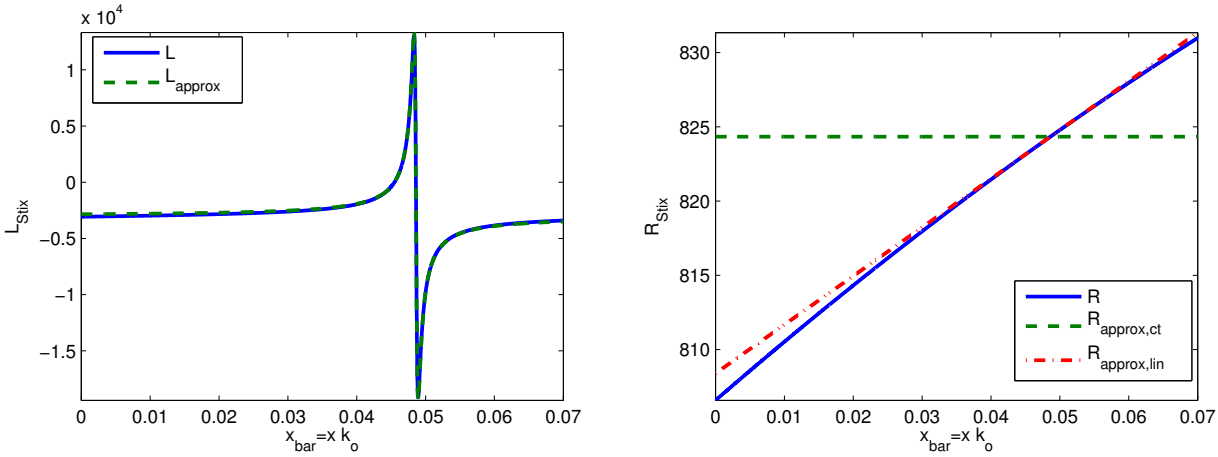

Figure 4: Plot of Stix's L and R coefficients as well as their approximations.

Labeling

$$R_o = 1 - \sum_{\beta:e,maj,min} \frac{\omega_{p,\beta}^2(x_{min})}{\omega[\omega + \Omega_\beta(x_{min})]}$$

$$L_o = 1 - \sum_{\beta:e,maj} \frac{\omega_{p,\beta}^2(x_{min})}{\omega[\omega - \Omega_\beta(x_{min})]}$$

$$L_1 = \frac{\omega_p^2(x_{min})}{\omega^2} R_{min}$$

$$\xi = \frac{\nu R_{min}}{\omega}$$

we then can rewrite the above dispersion equation root compactly as

$$k_{\perp,FW}^2 = k_o^2 \frac{(R_o - n_{//}^2)(L_o - L_1/(x+i\xi) - n_{//}^2)}{S_o - L_1/[2(x+i\xi)] - n_{//}^2}$$

$$= k_o^2 \frac{(R_o - n_{//}^2)([L_o - n_{//}^2](x+i\xi) - L_1)}{[S_o - n_{//}^2](x+i\xi) - L_1/2}$$

upon defining $S_o = (R_o + L_o)/2$ and where $n_{//} = k_{//}/k_o$. The approximate differential equation is then

$$\Big[[S_o - n_{//}^2](x+i\xi) - \frac{L_1}{2}\Big]\frac{dE_y^2}{d^2x} + k_o^2\Big[[R_o - n_{//}^2][L_o - n_{//}^2](x+i\xi) - L_1[R_o - n_{//}^2]\Big]E_y = 0$$

which is of the generic form

$$[a_{20} + a_{21}x]\frac{dE_y^2}{d^2x} + [a_{00} + a_{01}x]E_y = 0 \tag{1}$$

with

$$a_{20} = -\frac{L_1}{2} + i\xi[S_o - n_{//}^2]$$

$$a_{21} = [S_o - n_{//}^2]$$

$$a_{00} = k_o^2\Big[- L_1[R_o - n_{//}^2] + i\xi[R_o - n_{//}^2][L_o - n_{//}^2]\Big]$$

$$a_{01} = k_o^2[R_o - n_{//}^2][L_o - n_{//}^2]$$

Provided both a_{01} and a_{21} are nonzero, the above is readily written as a Budden equation

$$\frac{d^2E_y}{d\tilde{X}^2} + [1 - \frac{\eta}{\tilde{X}}]E_y = 0$$

where

$$\tilde{X} = \frac{a_{01}^{1/2}}{a_{21}^{3/2}}[a_{20} + a_{21}x] \tag{2}$$

and

$$\eta = \frac{a_{01}a_{20} - a_{00}a_{21}}{a_{21}^{3/2}a_{01}^{1/2}}$$

The just found approximate equation is suitable close to the minority cyclotron layer but is not sufficiently accurate close to the second ion-ion hybrid layer, located on the high magnetic field side of the ^3He cyclotron resonance. Adopting a similar procedure as before we can write an approximate dispersion as

$$k_{\perp,FW}^2 = k_o^2 \frac{(R_o - n_{//}^2 - R'x_S)(L_o - n_{//}^2 - L'x_S) + [L'(R_o - n_{//}^2 - R'x_S) + R_1(L_o - n_{//}^2 - L'x_S)]x}{S'(x - x_S)}$$

where x_S is the position where $S = n_{//}^2$ and

$$R_o = 1 - \sum_{\beta:e,maj,min} \frac{\omega_{p,\beta}^2(x_S)}{\omega[\omega + i\nu + \Omega_\beta(x_S)]}$$

$$R' = -\sum_{\beta:e,maj,min} \frac{\omega_{p,\beta}^2(x_S)}{\omega[\omega + i\nu + \Omega_\beta(x_S)]}[\frac{N_e'}{N_e} + \frac{\Omega_\beta}{R(x_S)(\omega + i\nu + \Omega_\beta)}]$$

$$L_o = 1 - \sum_{\beta:e,maj,min} \frac{\omega_{p,\beta}^2(x_S)}{\omega[\omega + i\nu - \Omega_\beta(x_S)]}$$

$$L' = -\sum_{\beta:e,maj,min} \frac{\omega_{p,\beta}^2(x_S)}{\omega[\omega + i\nu - \Omega_\beta(x_S)]}[\frac{N_e'}{N_e} - \frac{\Omega_\beta}{R(x_S)(\omega + i\nu - \Omega_\beta)}]$$

$$S' = \frac{R' + L'}{2}$$

The relevant approximate differential equation is now of the same form as Eq.1 but

$$a_{20} = -S' x_S$$
$$a_{21} = S'$$
$$a_{00} = k_o^2 (R_o - n_{//}^2 - R' x_S)(L_o - n_{//}^2 - L' x_S)$$
$$a_{01} = k_o^2 \Big[L'(R_o - n_{//}^2 - R' x_S) + R'(L_o - n_{//}^2 - L' x_S) \Big]$$

and can also be written as a Budden equation. More easily and general, but anticipating that the region of interest has a cutoff and a resonance, the dispersion equation roots can be approximated by

$$k_\perp^2 \approx \frac{a(x - x_{res}) + b}{x - x_{res}} = \frac{a(x - x_{cut})}{x - x_{res}}$$

where x_{res} is the location of the fast wave resonance i.e. $S(x_{res}) = n_{//}^2$ and x_{cut} is the position of the $R - n_{//}^2$-cutoff close to resonance, one readily finds

$$a = + \frac{dk_\perp^2(x_{cut})}{dx}(x_{cut} - x_{res})$$
$$b = - \frac{dk_\perp^2(x_{cut})}{dx}(x_{cut} - x_{res})^2.$$

Looking at the expression, it is also seen that a is the asymptotic value of n^2. Identifying the coefficients as done above, one gets

$$\eta = -b/a^{1/2} = a^{1/2}(x_{cut} - x_{res}) = k_{\perp,\infty}^2 \Delta x = [\frac{dk_\perp^2(x_{cut})}{dx}]^{1/2}(x_{cut} - x_{res})^{3/2}.$$

Figure 5 depicts the fast wave dispersion equation root and its approximate expressions adopting the local approximations of the dispersion equation for 3 different H majority concentrations. Crudely speaking, the dispersion equation roots in the region of interest can thus be approximated by a sequence of 3 regions, 2 of which are described by Budden's equation and the third - a usually small region connecting the two interaction regions - where the wavelength can be assumed not to change at all. The solutions in the latter transfer region are simply of the form $exp[\pm ikx]$. Figure 6 sketches the approximate dispersions in the 3 regions of interest. If the region is somewhat wider, this approximation may be too crude and a more suitable equation allows for a small variation of the wavelength so that $d^2E/dx^2 + (ax + b)E = 0$ is more appropriate. This equation can be reduced to the Airy

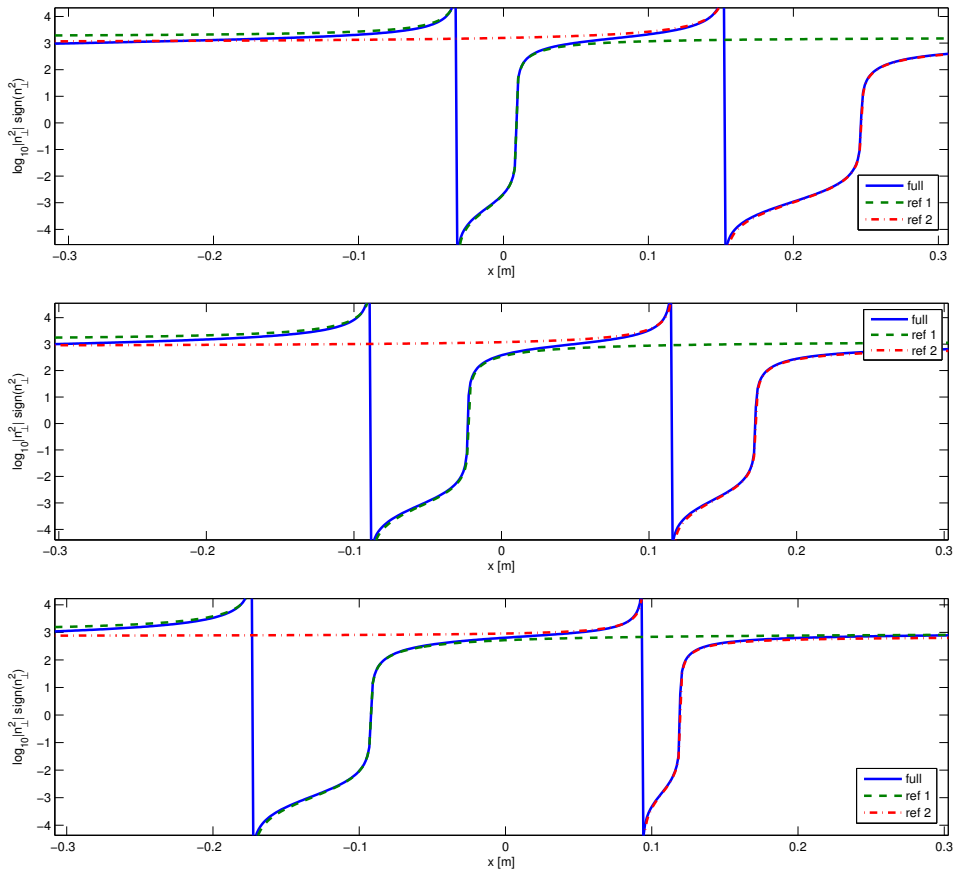

Figure 5: Square of the perpendicular refractive index found solving the fast wave cold plasma dispersion equation, and local dispersion root fit for $X[H] = 62\%$, $X[H] = 67\%$ and $X[H] = 72\%$.

equation $d^2E/dz^2 + zE = 0$ by the transformation $z = \alpha x + \beta$ in which $\alpha = a^{1/3}$ and $\beta = b/a^{2/3}$, the solutions of which solutions are of the approximate form $z^{-1/4}exp[\pm i2/3z^{3/2}]$ well away from the cutoff $x = -b/a$ (the cutoff is already included in the Budden description).

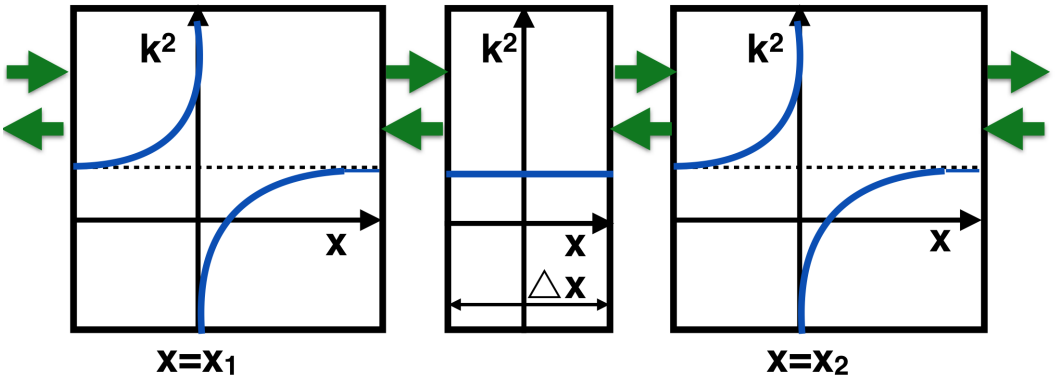

Figure 6: Qualitative sketch of the sequence of layers the wave tunnels through.

The subdivision into the 3 subregions is somewhat arbitrary: strictly, the distance away from

the confluence region should be large enough to allow the solution to be well approximated by the leading term of the asymptotic solution of the simplified equation which will be used to find the connection coefficients. But at that point, the actual dispersion root is different from that of the simplified model. Likewise, in the region connecting the 2 resonance-cutoff zones, the dispersion equation root is varying nonlinearly. Figure 7 plots the resonance-cutoff distances η_A and η_C as well as the width of the connection region $\Delta_{x,B}$ for a wide range of ^3He minority and H majority concentrations; the transition region is assumed to have a width of 75% of the distance between the leftmost cutoff and the rightmost resonance and the connection points are defined symmetrically w.r.t. these points.

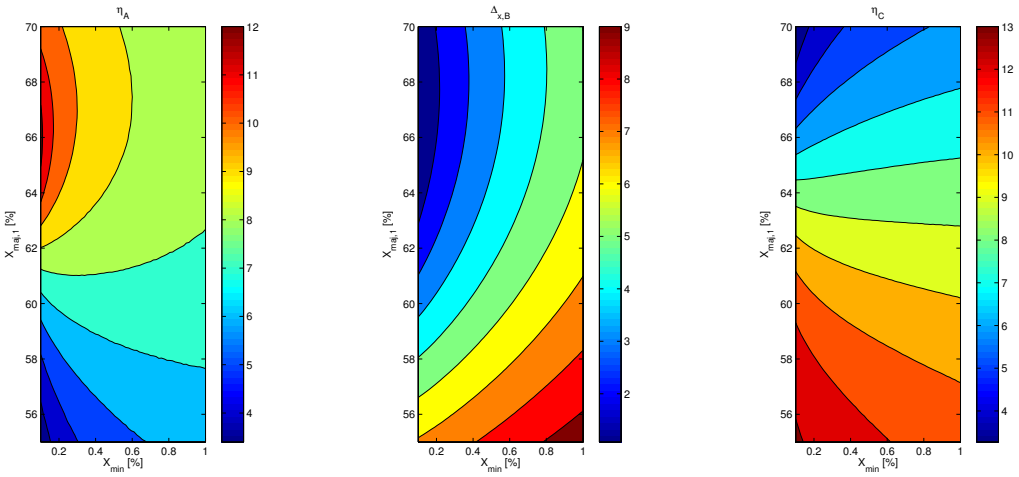

Figure 7: Resonance-cutoff distances and distance between the 2 interaction regions.

The next task is to find solutions in each of the regions and connect the various solutions requiring the field and its derivative are continuous at the boundaries. The discussion of the solution of Budden's equation is done in the next section.

4 Finding the relevant connection coefficients

In the previous section it was found that classical equations allow to capture the behaviour of the E_y field component relevant for the 3-ion heating scheme: Budden's equation which is characterised by a back-to-back resonance/cutoff pair ($d^2E_y/d\tilde{X}^2 + [1 - \eta/\tilde{X}]E_y = 0$), and Airy's equation ($d^2E_y/d\tilde{X}^2 + \tilde{X}E_y = 0$) for which grows linearly with distance. If the variation of $k_\perp^2$ is neglected, Airy's equation can be substituted for the even simpler equation for which $k_\perp^2$ is a constant. For the latter case, the solutions are simple plane waves $E_y = exp[\pm i\tilde{X}]$. For the other two equations, the reflection and transmission coefficients can be found relying on the method of Laplace. As both equations have been studied in the literature, their solutions are well know. The interested reader is referred to the Appendix for details on the evaluation of the connection coefficients.

The asymptotic solution of Budden's equation that propagates towards growing $\tilde{X}$ is

$$E_{y,k\approx 1} = exp[i\tilde{X}]2^{-i\eta/2-1}\int_{contour} d\tilde{k} exp[i\tilde{k}\tilde{X}]\tilde{k}^{i\eta/2-1}$$

while that propagating towards decreasing $\tilde{X}$ is the complex conjugate of the above. For incidence from either side the transmission is $T = exp(-\pi\eta/2)$. For incidence from the side of the resonance the reflection coefficient is zero while incidence from the side of the cutoff yields $R = 1 - exp(-\pi\eta)$. The corresponding fluxes are $T_F = exp[-\pi\eta]$ and $R_F = (1 - exp[-\pi\eta])^2$. In the former case the absorption is $1 - T_F$ while in the latter case it is $T_F(1 - T_F)$.

The solutions of Airy's equation are

$$E \approx \frac{\pi^{1/2}}{\tilde{X}^{1/4}} exp[\pm i(\frac{2}{3}\tilde{X}^{3/2} - \frac{\pi}{4})].$$

In the present application the cutoff does no lie in the domain of interest and hence the decoupled modes remain decoupled. In case one of the resonance pairs is replaced by an isolated cutoff, the connection coefficients are as follows: For incidence from the evanescent side, the same WKB mode contributes at both sides of the cutoff so there is no reflection when approaching from the evanescent side. For incidence on the cutoff from the propagative side, a contribution of the outward propagating mode is picked up. Both WKB modes have the same amplitude when $\tilde{X} >> 0$ but the reflection coefficient is dephased by $\pi/2$.

When solving the equation for 2 sets (E_1, E_2) of independent boundary conditions the coefficients (α_1, α_2) of a general solution $E_G = \alpha_1 E_1 + \alpha_2 E_2$ can be found by solving

$$\begin{pmatrix} E_G \\ dE_G/d\tilde{X} \end{pmatrix} = \begin{pmatrix} E_1 & E_2 \\ dE_1/d\tilde{X} & dE_2/d\tilde{X} \end{pmatrix} \cdot \begin{pmatrix} \alpha_1 \\ \alpha_2 \end{pmatrix}$$

Two simple independent equations can be found imposing $E = 1$ at the left end of the interval and $E = 0$ at the right end, and vice versa. Away from the interaction region, the eigensolutions of the equation can written as $exp[\pm i\tilde{X}]\tilde{X}^{\mp i\eta/2}/exp[\pm\beta\eta/2]$ in which β is the argument of $\tilde{X}$. As $\tilde{X}$ is to be interpreted as $\tilde{X} + i\nu$ with ν very small and positive, $\beta = \pi$ when $\tilde{X} < 0$; it is 0 for positive $\tilde{X}$.

The finite collision frequency ν substitutes resonances by quasi-resonances i.e. regions where the solution has steep but finite gradients and eases numerical cross-checking of the obtained results. Figure 8 depicts the numerically found solutions of the Budden equation for $\eta = 0.5$ and $\nu = 10^{-2}$. The transmission and reflection coefficients are in good agreement with the analytical limit $\nu \to 0^+$ yielding $T = 0.46$ and $R = 0.79$ for the amplitudes and the squares of these numbers $T = 0.21$ and $R = 0.63$ for the fluxes.

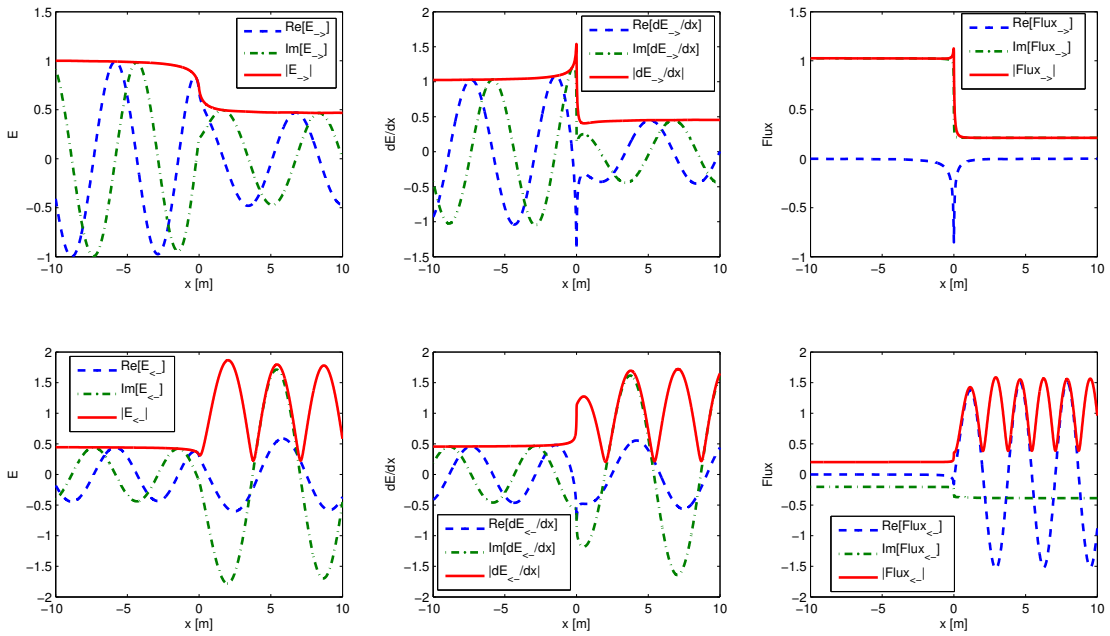

Figure 8: Solutions for incidence from the left (top) and incidence from the right (bottom): electric field (left), derivative of the field (middle) and flux (right).

From the connection coefficients we can construct a transfer matrix. Linking the eigenvector solutions s_1 and s_2 on the left and on the right of the interaction region we have

$$\begin{pmatrix} s_{1,L} \\ s_{2,L} \end{pmatrix} = \begin{pmatrix} \alpha_{11} & \alpha_{12} \\ \alpha_{21} & \alpha_{22} \end{pmatrix} . \begin{pmatrix} s_{1,R} \\ s_{2,R} \end{pmatrix} = \overline{\overline{N}}_{\eta} . \begin{pmatrix} s_{1,R} \\ s_{2,R} \end{pmatrix}$$

i.e.

$$\begin{pmatrix} 1 \\ 0 \end{pmatrix} = \begin{pmatrix} \alpha_{11} & \alpha_{12} \\ \alpha_{21} & \alpha_{22} \end{pmatrix} . \begin{pmatrix} T \\ 0 \end{pmatrix}$$

for incidence from the left and

$$\begin{pmatrix} 0 \\ T \end{pmatrix} = \begin{pmatrix} \alpha_{11} & \alpha_{12} \\ \alpha_{21} & \alpha_{22} \end{pmatrix} . \begin{pmatrix} 1 - T^2 \\ 1 \end{pmatrix}$$

for incidence from the right where $T = exp[-\pi\eta/2]$. This yields

$$\overline{\overline{N}}_\eta = \begin{pmatrix} T^{-1} & T - T^{-1} \\ 0 & T \end{pmatrix}$$

The transfer matrix in a region of width $\Delta\tilde{X}$ away from the resonance i.e. where $k_\perp^2 \approx 1$ is constant is simply

$$\begin{pmatrix} s_{1,L} \\ s_{2,L} \end{pmatrix} = \begin{pmatrix} e^{-i\Delta\tilde{X}} & 0 \\ 0 & e^{+i\Delta\tilde{X}} \end{pmatrix} \cdot \begin{pmatrix} s_{1,R} \\ s_{2,R} \end{pmatrix} = \overline{\overline{N}}_{\Delta x} \cdot \begin{pmatrix} s_{1,R} \\ s_{2,R} \end{pmatrix}$$

where now simply $s_1 = exp[+i\tilde{X}]$ and $s_2 = exp[-i\tilde{X}]$ (substituted by $exp[\pm 2i/3\tilde{X}^{3/2}]/\tilde{X}^{1/4}$ if accounting for the modest change of $k_\perp^2$ in the transition region).

To connect the 3 regions together we need to impose the continuity of E and $dE/d\tilde{X}$ at each connection point. We now need to account for the fact that $\tilde{X} = 0$ was defined to be the resonance position in each of the resonance regions. Labeling the leftmost Budden region as "A", the intermediate region as "B" and the rightmost Budden region as "C", we have

$$s_{1,A}(\tilde{X}) = e^{+i[\tilde{X} - \tilde{X}_A]}(\tilde{X} - \tilde{X}_A)^{-i\eta_A/2}$$
$$s_{2,A}(\tilde{X}) = e^{-i[\tilde{X} - \tilde{X}_A]}(\tilde{X} - \tilde{X}_A)^{+i\eta_A/2}$$

in the interval $[\tilde{X}_L - \tilde{X}_{c,1}]$ containing $\tilde{X}_A$,

$$s_{1,B}(\tilde{X}) = e^{+i\tilde{X}}$$
$$s_{2,B}(\tilde{X}) = e^{-i\tilde{X}}$$

(or its Airy-function upgrade) in the interval $[\tilde{X}_{c,1} - \tilde{X}_{c,2}]$ of width $\Delta\tilde{X}_B$,

$$s_{1,C}(\tilde{X}) = e^{+i[\tilde{X} - \tilde{X}_C]}(\tilde{X} - \tilde{X}_C)^{-i\eta_C/2}$$
$$s_{2,C}(\tilde{X}) = e^{-i[\tilde{X} - \tilde{X}_C]}(\tilde{X} - \tilde{X}_C)^{+i\eta_C/2}$$

in the interval $[\tilde{X}_{c,2} - \tilde{X}_R]$ containing $\tilde{X}_C$. Rather than using the above eigenvectors, a normalised version needs to be used to ensure that the sum of all outgoing fluxes and the loss of flux at the resonances adds up to the incoming flux. Recalling that the simplified wave equation is modelling the fast wave, the relevant flux is the renormalised Poynting flux:

$$\mathtt{F} = \frac{1}{2\mu_o} Re[E_y^* \frac{1}{i\omega} \frac{d}{d\tilde{X}} E_y] = \frac{1}{2\mu_o \omega} Im[E_y^* \frac{d}{d\tilde{X}} E_y].$$

At the first interface $\tilde{X} = \tilde{X}_{c,1}$, continuity of the field and its derivative can be imposed using

$$\overline{\overline{M}}_A . \begin{pmatrix} \alpha_{1,A} \\ \alpha_{2,A} \end{pmatrix} = \begin{pmatrix} E \\ dE/d\tilde{X} \end{pmatrix} = \overline{\overline{M}}_B . \begin{pmatrix} \alpha_{1,B} \\ \alpha_{2,B} \end{pmatrix}$$

i.e.

$$\begin{pmatrix} \alpha_{1,A} \\ \alpha_{2,A} \end{pmatrix} = \overline{\overline{M}}_A^{-1} . \overline{\overline{M}}_B . \begin{pmatrix} \alpha_{1,B} \\ \alpha_{2,B} \end{pmatrix} = \overline{\overline{C}}_{AB} . \begin{pmatrix} \alpha_{1,B} \\ \alpha_{2,B} \end{pmatrix}.$$

Here $\overline{\overline{M}}_\mu$ is the local eigenvector matrix

$$\overline{\overline{M}}_\mu = \begin{pmatrix} s_{1,\mu} & s_{2,\mu} \\ ds_{1,\mu}/d\tilde{X} & ds_{2,\mu}/d\tilde{X} \end{pmatrix}$$

where the s_α are the eigenvectors corrected for the flux factor $1/|\mathtt{F}|^{1/2}$ adjusting the amplitude consistent with the change of $k_\perp^2$ across the interval in absence of damping. The same is done at the second interface. The whole transfer matrix $\overline{\overline{N}}_{tot}$ is then found connecting the leftmost and rightmost coefficients assembling all the above. One gets

$$\begin{pmatrix} \alpha_{1,L} \\ \alpha_{2,L} \end{pmatrix} = \overline{\overline{N}}_{tot} . \begin{pmatrix} \alpha_{1,R} \\ \alpha_{2,R} \end{pmatrix} = \overline{\overline{N}}_{\eta_A} . \overline{\overline{C}}_{AB} . \overline{\overline{N}}_{\Delta\tilde{X}} . \overline{\overline{C}}_{BC} . \overline{\overline{N}}_{\eta_C} . \begin{pmatrix} \alpha_{1,R} \\ \alpha_{2,R} \end{pmatrix}$$

For incidence from the left ($(s_{1,L}, s_{2,R}$=(1,0)) the relevant system is the transmission and reflection coefficients in terms of the above eigenvectors are

$$T = \frac{1}{N_{tot,1,1}}$$
$$R = \frac{N_{tot,2,1}}{N_{tot,1,1}}$$

and for incidence from the right

$$T = \frac{N_{tot,1,1}N_{tot,2,2} - N_{tot,1,2}N_{tot,2,1}}{N_{tot,1,1}}$$

$$R = -\frac{N_{tot,1,2}}{N_{tot,1,1}}$$

Figure 9 depicts the total absorption in the region containing the 2 sets of resonance-cutoff pairs and the transit region for a set of relevant parameters, η_A, Δx_B and η_C computed from the Stix coefficient approximations for the case that waves are incident from the right. Remind that the transformation from the approximate wave equation to the Budden equation brings in a scale reduction, the refractive index being of order 30. All 3 parameters play a role but as it requires a significant part of the power to get up to that point, the leftmost interaction layer lying further from the point of incidence has a somewhat more modest role than the other 2 parameters. Figure 9 reproduces the characteristic multiple optimal damping regions found numerically by Kazakov when scanning over the minority and majority concentrations [2] but retaining kinetic effects so that the actual damping is described rather than a mock-up, as is done here. Since many details of the dynamics are glossed over by the approximate model, the results are reproduced qualitatively rather than quantitatively. In particular, the differing damping efficiency depending on whether ion or electron damping - or a combination - takes place is out of the scope of the present model where all "damping" occurs at the resonances. The dispersion equation roots depicted in Fig. 5 show that the width of the transit region Δx_B varies significantly when the majority concentration is changed. The successive peaks in the double transit absorption coefficient are a consequence of the constructive and destructive interference of the incident, transmitted and reflected waves.

This effect was first noted by Fuchs and Bers [9] who demonstrated that the fast wave mode conversion efficiency described by the tunneling equation (see e.g. [10]) can be increased from the "single transit" value of maximally 25% to 100% by accounting for the fact that power transmitted through the interaction region proceeds to the high field side $R - n_{//}^2$ cutoff and is reflected there. The wave proceeds back to the confluence region and hits the interaction region a second time, giving rise to wave interference. In particular, it was demonstrated that if an integer number of wavelengths can be folded between the cutoff and the confluence, the mode conversion efficiency is dramatically boosted.

The role of such interference has been noted experimentally, e.g. during ^{3}He minority experiments in D plasmas on JET [11]. Later, a similar effect was observed during (^{3}He)-H heating experiments in JET plasmas, where wave interference was caused by the appearance of the second mode conversion layer due to the plasma contamination with carbon impurities [6]. Making use of Stokes and anti-Stokes lines, the wave interference effect was examined for mode conversion heating in [12]. This effect is identified in the present paper to be a significant player in the 3-ion scheme when most of incident RF power is absorbed by minority ions rather than by electrons as in mode conversion experiments. The interference described by Fuchs and Bers is described by the isolated high field side R-cutoff. The 3-ion-scheme

equally benefits from a similar wave interference but does so for interaction regions lying closer to each other; rather than the R-cutoff, the resonance-(L)-cutoff pair occurs here. A discussion of the kinetic collisionless damping effects deciding on whether the power is ultimately absorbed by ions or electrons is outside the scope of the present paper. However, we note that since low minority concentrations are adopted in this scenario, the IIH layer stays sufficiently close to the cyclotron resonance of minority ions, which is favourable for wave damping on ions. This observation is supported by the results of more sophisticated 1-D and 2-D full-wave modelling presented earlier [2]. Whereas the common strategy to ensure optimal damping of a desired species requires ensuring that the wave has the proper polarisation at the location where the desired type of damping is efficient, the 3-ion scheme additionally profits from the wave interference to maximise efficiency.

The results presented here are idealised in various respects: (i) They isolate a single parallel wave number whereas the spectrum launched from RF waves contains multiple components. (ii) The metallic tokamak vessel acts as a Faraday cage so that waves launched from the antennas execute multiple passes over the plasma before being damped in case the core damping scheme is not very efficient; for full rigour parasitic damping in the edge should be included to have a better idea of how and where the launched power is absorbed. (iii) A 1D description is used while the actual geometry is 3-dimensional; wave diffraction in the tokamak plasma is not captured by the adopted model. Past JET-C experiments focused on usual minority heating and mode conversion heating [6, 11] show that the effect of the interference remains but it is more complex and less sharply de fined. Recent JET and C-Mod experiments exploring the 3-ion scheme [3, 4, 5] showed a rather high efficiency of plasma heating for a fairly broad range of the isotopic ratio and ^3He concentrations. This is also related to the fact that once the tail of energetic minority ions builds up, the efficiency of wave damping generally increases [13].

5 Alternative approach for the cyclotron layer

The previous section points out that the effects observed in the 3-ion scheme come about by wave interference brought about by reflected waves from interaction regions modeled by the Budden equation, one region modelling the ion-ion hybrid layer associated with the majority ions, and the other with the 3rd species, the small minority. Strong reflection can equally be obtained from regions with steep gradients. In the particular scenario studied here, such steep gradients are brought about by the presence of the minority cyclotron layer and the localised damping associated with it, as is demonstrated in the accompanying paper [14]. In the limiting case where the damping is only at the cyclotron layer itself, the $k_\perp^2$ in the second order differential wave equation for E_y can be interpreted as $k_\perp^2 + i\alpha\delta(x - x_{min})$. Integrating the differential equation across the cyclotron resonance allows finding that the derivative of E_y satisfies the jump condition

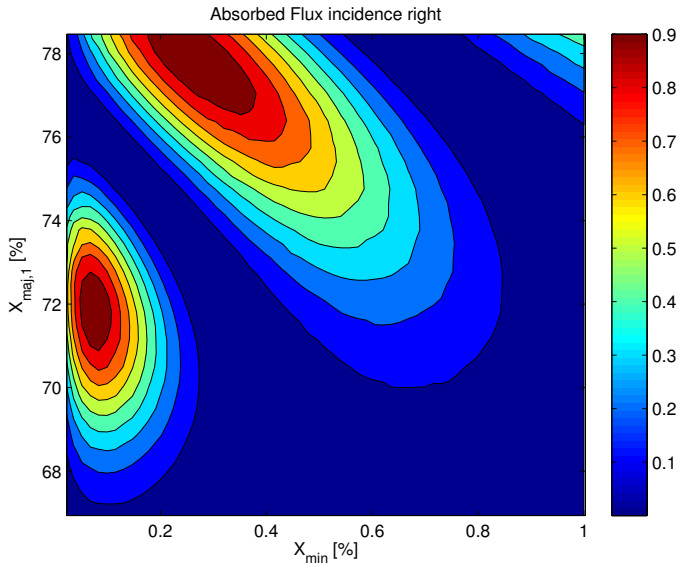

Figure 9: Resonant absorption as a function of the majority H and minority ^3He concentration adopting the simplified differential equations and the analytically obtained connection coefficients.

$$[[\frac{d}{dx}E_y]]|_{x=x_{min}} = -i\alpha E_y|_{x=x_{min}}$$

where [[...]] denotes the jump. E_y itself being continuous one readily finds that at the cyclotron layer and for incidence from either side the transmission and reflection coefficients are

$$T = \frac{1}{1+\zeta}$$
$$R = -\frac{\zeta}{1+\zeta} exp[2ik_\perp x_{min}]$$

in which $\zeta = \alpha/[2k_\perp]$, it can easily be seen that when the damping disappears, the corresponding reflection dies away and the transmission is complete. The corresponding connection matrix is

$$\overline{\overline{M}}_B = \begin{pmatrix} T^{-1} & -RT^{-1} \\ RT_{-1} & T - R^2T^{-1} \end{pmatrix},$$

which can be used instead of the earlier formulated one when clicking the solutions in the various regions together.

Whereas the Budden model identifies the resonance layer as the location where the fast wave loses its energy, the delta function description places it at the location where the minority damping actually takes place: at the minority layer. This ambiguity is at the origin of the incapacity of fast-wave-only models to give a rigorous account on which species ultimately benefit from the incoming and locally damped wave heating power and why a proper description of the finite Larmor radius effects is necessary. Kinetic modelling (see e.g. [15, 16]) shows that the Budden wave resonance is the 1-wave-only mock-up of a confluence to a short wavelength branch and that efficient electron damping is taking place close to the conversion point on this short wavelength branch. It equally shows that Doppler broadening widens the cyclotron resonance. Hence, both ion and electron damping typically take place in the interaction region. Dispersion equation studies show that the proximity of the confluence, cutoff and cyclotron layer give rise to overlapping of coupling and damping regions (see e.g. [17] in which mode conversion and damping is studied solely based on dispersion root evaluation) which can at best qualitatively be captured by simplified 1-wave models. Aside from lacking a proper description of the actual damping mechanisms, a straightforward reason of why the constructive-destructive interference effects described in this paper can not fully capture the wave physics is that fact that *asymptotic* solutions are matched while (i) none of the solutions has actually reached its asymptotic regime, the proximity of 2 interaction regions being a base ingredient of the 3-ion scheme, and (ii) even the correct mathematical solutions of the simplified equations do not do justice to the actual intricate full wave behaviour.

6 Conclusions

The 3-ion heating scheme's [2] heating efficiency is studied analytically using cold plasma modelling. We show that high efficiency of the double transit absorption can be achieved due to wave interference effects. This effect was first identified by Fuchs and Bers [9] and generalised later by Kazakov [12]. Here, we study the case of two back-to-back mode conversion layers existing due to the presence of three ion species rather than just two. One of the ion-ion hybrid layers lies close to the fundamental cyclotron layer of the minority, the second one can be moved sufficiently close to the first by adequately choosing the relative concentrations of the majority ions. As is the case for the usual minority heating scheme, the proximity of the resonance layer affects the polarisation, the proper tuning of the latter being a key ingredient in maximising the absorption in more sophisticated kinetic models.

7 Acknowledgements

This work has been carried out within the framework of the EUROfusion Consortium and has received funding from the Euratom research and training programme 2014-2018 under

grant agreement No 633053. The views and opinions expressed herein do not necessarily reflect those of the European Commission.

Appendix: Asymptotic solutions of the Budden and Airy equations

The Budden and Airy equations both are classical equation (see e.g. [18] and [19]).) and their solutions are well known so the connection formulae obtained in the present section are mere reminders. For finding the connection coefficients of the above equation the method of Laplace can be used (see e.g. [20] for the general principle, and the particularly elegant description in [21] for its application). For a differential equation with linear coefficients

$$\sum_n [a_n \tilde{X} + b_n] \frac{d^n G}{d\tilde{X}^n} = 0 \tag{3}$$

the solution can formally be written as an line integral in k-space:

$$G = \int_{contour} dk exp[ik\tilde{X}] V(k) dk.$$

Introducing this into the differential equation and assuming that end contributions to the line integral vanish, one readily finds that the function V has to satisfy

$$\sum_n \left[[b_n (ik)^n + i a_n \frac{d}{dk} [(ik)^n]] V(k) + i a_n (ik)^n \frac{dV}{dk} \right] = 0$$

so that

$$G(x) = \int_{contour} dk \frac{exp[ik\tilde{X}]}{\sum_n a_n (ik)^n} exp[i \int dk' \frac{\sum_n b_n (ik')^n}{\sum_n a_n (ik')^n}] \tag{4}$$

Adopting this general procedure for differential equations with linear coefficients Eq.1 to the specific case of the Budden equation, the solution can be written

$$E_y = \int_{contour} dk exp[ik\tilde{X}] [k-1]^{i\eta/2-1} [k+1]^{-i\eta/2-1},$$

which is suitable to evaluate the solutions of the equation far away from the resonance and cutoff. Adopting the Hankel contour encircling the poles $k = \pm 1$ yields the independent solutions corresponding to the incoming and outgoing waves. A branch cut is associated with each of the asymptotic dispersion equation roots. To ensure that the dominant contribution comes from the close neighbourhood of the poles, the contours must start and end at large

$|k|$ at $k = |k|exp[i\pi/2]$ for large positive and at $k = |k|exp[-i\pi/2]$ for large negative x. Around $k = 1$ and for sufficiently large $|x|$, the above can be approximated by

$$E_{y,k\approx 1} = exp[i\tilde{X}]2^{-i\eta/2-1}\int_{contour} d\tilde{k}exp[i\tilde{k}\tilde{X}]\tilde{k}^{i\eta/2-1}.$$

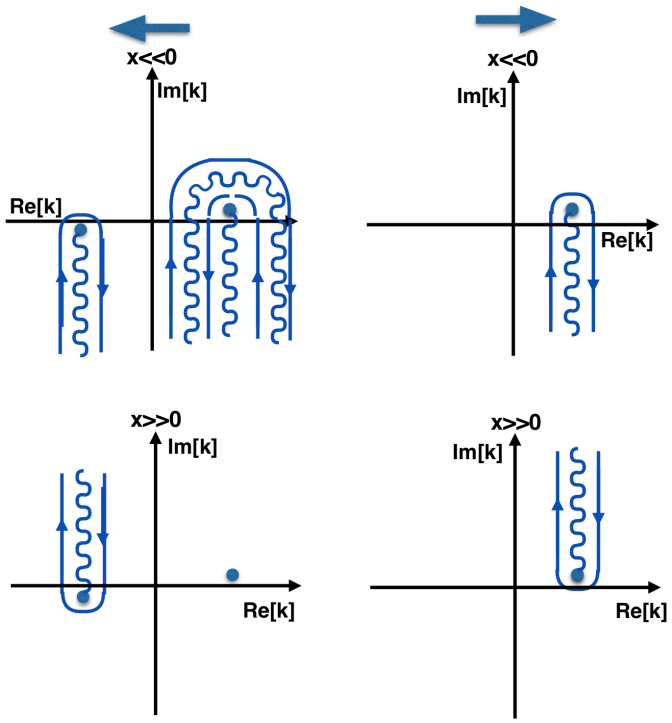

Figure 10: Contours adopted for representing the solutions of the Budden-type local differential equation.

in which the integral is the Hankel integral [20],

$$G(\alpha, \tilde{X}) = \int dkk^{\alpha}exp[ik\tilde{X}]$$

which evaluated in the principal Riemann sheet has the value

$$G(\alpha, \tilde{X}) = \frac{2\pi i}{\Gamma(-\alpha)}(i\tilde{X})^{-(1+\alpha)}$$

hence

$$E_{y,k\approx 1} \approx -\frac{2\pi(2i)^{-i\eta/2-1}}{\Gamma(1-i\eta/2)}exp[i\tilde{X}]\tilde{X}^{-i\eta/2} = Cexp[i\tilde{X}]\tilde{X}^{-i\eta/2}.$$

The complex conjugate of this solution $C^* exp[-i\tilde{X}]\tilde{X}^{+i\eta/2}$ is the solution corresponding to the contour integral encircling $k \approx -1$.

To find the analytical continuations of the solutions, it is sufficient to deform the contour by rotating it. For the wave that is incident from the side of the resonance, only an amplitude correction factor is found. For the solution incident from the side of the cutoff, a contribution from the other wave is picked up. For the wave amplitude one obtains the transmission coefficient $T_E = exp[-\pi\eta/2]$ for incidence from either side. For incidence from the side of the resonance the reflection is zero; from the other side $R_E = 1 - exp[-\pi\eta]$. The corresponding fluxes are $T_F = exp[-\pi\eta]$ and $R_F = (1 - exp[-\pi\eta])^2$. In the former case the absorption is $1 - T_F$ while in the latter case it is $T_F(1 - T_F)$.

For a forward wave, causality requires that $Im(k)$ has the same sign as $Re(k)$. For the Budden wave this requires that x is to be interpreted as $\tilde{X} + i\Delta$ where Δ is positive (the resonance lying slightly under the real axis i.e. $arg(\tilde{X}) = \pi$ when $\tilde{X} < 0$) when $\eta > 0$ and negative when $\eta < 0$. To the left of the resonance, $\tilde{X}^{-i\eta/2} = |\tilde{X}|^{-i\eta/2} exp[\pi\eta/2]$ so that the rightgoing wave amplitude is depleted by $T_E = exp[-\pi\eta/2]$ when crossing the resonance region. A summary of the connection coefficients is given in Fig. 11.

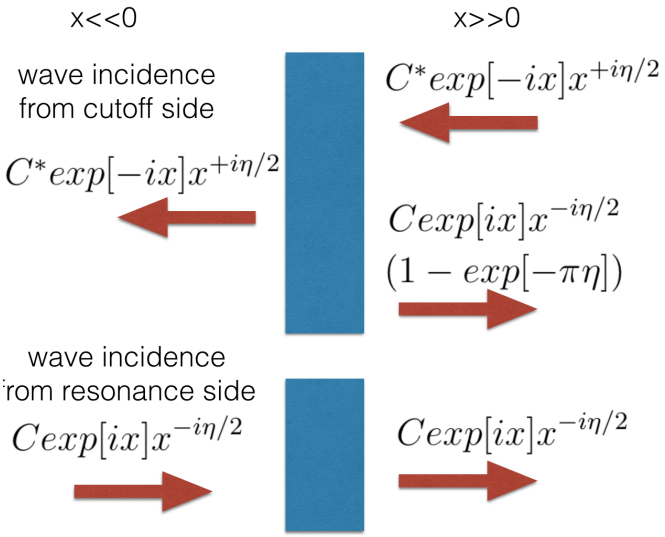

Figure 11: Connection coefficients for wave incidence from either the cutoff or the resonance side.

The line integral deformation method can equally be applied to the Airy equation $E'' + \tilde{X}E = 0$. Finding the proper coefficients by looking at the general expression Eq. 3, the contour integral equation Eq. 4 is

$$E = \int_{contour} dk exp\Big(i[k\tilde{X} - \frac{k^3}{3}]\Big) = \int_{contour} dk exp[G(k, \tilde{X})]$$

The WKB solutions at large $|\tilde{X}|$ can be found evaluating the above integral for path in the

complex k-plane passing through the saddle points $k_{SP} = \pm\tilde{X}^{1/2}$ and starting and ending in one of the 3 directions where the integrand dies away fast. If we label the argument of k as ξ, then at large $|k|$ the integrand is of the form

$$exp[-i\frac{|k|^3}{3}cos(3\xi)]exp[\frac{|k|^3}{3}sin(3\xi)]$$

so that ξ needs to be $\xi = \pi/2 + 2\pi M/3$ where M is an integer when $|k|$ approaches infinity to ensure fast decay of the integrand. Writing a Taylor series expansion of the function G near the saddle points one readily finds

$$E \approx exp[G(k_{SP}, \tilde{X})] \int_{contour} dk exp[\frac{1}{2}G''(k - k_{SP})^2].$$

Rotating the path by a change of variable $p = (-G''/2)^{1/2}(k - k_s)$ the integral can be evaluated, yielding

$$E \approx exp[G(k_{SP}, \tilde{X})](-\frac{2\pi}{G''})^{1/2} = \frac{\pi^{1/2}}{\tilde{X}^{1/4}} exp[\pm i(\frac{2}{3}\tilde{X}^{3/2} - \frac{\pi}{4})].$$

where the argument of $k - k_{SP}$ is $-\pi/4$ or $+\pi/4$ for $k_{SP,1} = \tilde{X}^{1/2}$ and $k_{SP,2} = -\tilde{X}^{1/2}$, respectively, when $\tilde{X} > 0$, and $-\pi/2$ and 0 when $\tilde{X} < 0$. Figure 12 depicts where the saddle point contributions are picked up and how the paths are deformed when going from $\tilde{X} << 0$ to $\tilde{X} >> 0$. For incidence from the left, the same WKB mode contributes at both sides of the cutoff (no reflection when approaching from the evanescent side). For incidence from the right, a contribution of the rightward propagating mode is picked up. As both WKB modes have the same amplitude when $\tilde{X} >> 0$, the reflection coefficient has unity amplitude but is dephased by $\pi/2$.

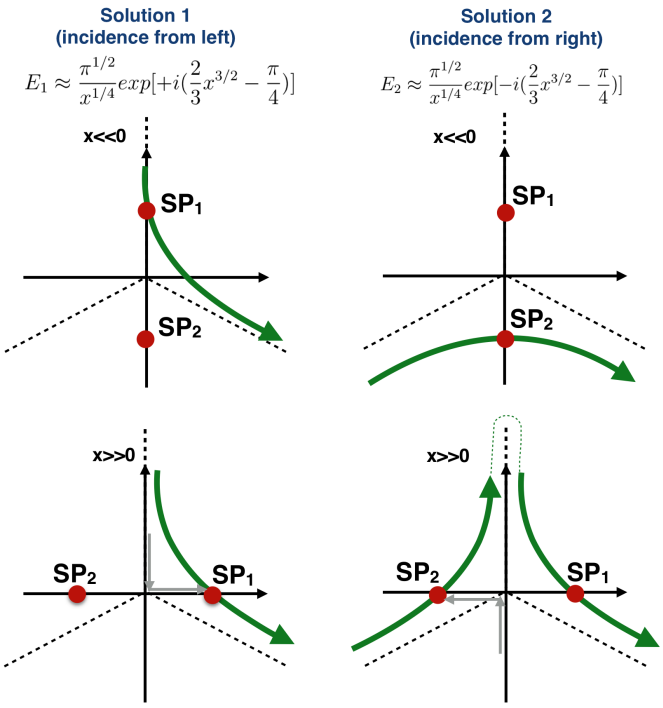

Figure 12: Contours adopted for representing the solutions of the Airy-type local differential equation.

References

[1] Ye.O. Kazakov et al, *Proc. 21st Topical Conference of Radio Frequency Power in Plasmas*, AIP Conf. Proc. **1689** (2015) 030008

[2] Ye.O. Kazakov et al., *Nucl. Fusion* **55** (2015) 032001

[3] Ye.O. Kazakov et al., *Experimental evidence for a novel method of fast-ion generation in multi-ion plasmas with RF waves*, in preparation for submission to *Physical Review Letters*

[4] X. Litaudon et al., *Overview of the JET results in support to ITER*, *Proc. 26th IAEA Fusion Energy Conference* (October 2016, Kyoto), paper OV/1-4

[5] J. Wright et al., *Experimental Results from Three-ion Species Heating Scenario on Alcator C-Mod*, *Proc. 26th IAEA Fusion Energy Conference*(October 2016, Kyoto), paper EXS/P3

[6] D. Van Eester et al., *Plasma Phys. Control. Fusion* **54** (2012) 074009

[7] T.H. Stix, *Waves in Plasmas* (1992) AIP, New York

[8] B.D. Fried and D.C. Conte, *The Plasma Dispersion Function: The Hilbert Transform of the Gaussian* (1961) Academic Press, New York and London.

[9] V. Fuchs et al., *Phys. Plasmas* **2** (1995) 1637-47

[10] D.G. Swanson, *Plasma Waves* (2003) IOP Publishing Ltd., London

[11] D. Van Eester et al., *Plasma Phys. Control. Fusion* **51** (2009) 044007

[12] Ye.O. Kazakov et al., *Plasma Phys. Control. Fusion* **52** (2010) 115006

[13] M. Schneider et al., *Nucl. Fusion* **56** (2016) 112022

[14] Ye.O. Kazakov et al., private communication; in preparation for submission

[15] M. Brambilla, *Plasma Phys. Control. Fusion* **1993** 3541

[16] D. Van Eester et al., *Plasma Phys. Contr. Fusion* **40** 11 (1998) 1949-1975

[17] R.R. Weynants et al., Proc. *4th Int. Symposium on Heating in Toroidal Plasmas*, Rome (1984) Vol. I, 211

[18] K.G. Budden, *Radio waves in the ionosphere* (1961) Cambridge University Press, Cambridge

[19] G.N. Watson, *A Treatise on the Theory of Bessel Functions* (1966) Cambridge University Press, Cambridge

[20] M. Abramowitz and I. Stegun, *Handbook of Mathematical Functions* (1972) Dover Publications, New York

[21] D. Gambier and J. Schmitt, *Phys. Fluids* **26** (1983) 2200